2021 International Aegean Conference on Electrical Machines and Power Electronics (ACEMP) & 2021 International Conference on Optimization of Electrical and Electronic Equipment (OPTIM) | 978-1-6654-0298-9/21/$31.00 ©2021 IEEE | DOI: 10.1109/OPTIM-ACEMP50812.2021.9590032

Extended Describing Function Modeling and Closed-Loop Control of LLC Converter in Battery Charging Applications

1st Abdulsamed Lordoglu
Department of Electrical Engineering
Istanbul Technical University
Istanbul, Turkey
lordoglu@yildiz.edu.tr

2nd Mehmet Onur Gulbahce
Dept. of Elec. and Electronics Engineering
Fatih Sultan Mehmet Vakif University
Istanbul, Turkey
mogulbahce@fsm.edu.tr

3rd Derya Ahmet Kocabas
Department of Electrical Engineering
Istanbul Technical University
Istanbul, Turkey
kocabasde@itu.edu.tr

4th Serkan Dusmez
R&D Department, Power Electronics
Arcelik Global
Istanbul, Turkey
serkan.dusmez@arcelik.com

***Abstract*—The variable switching frequency control of LLC converters makes the modeling and compensator design rather a difficult task. In this paper, an extended describing function modeling that can represent the beat frequency successfully has been examined in detail. The small signal model of the converter dynamics has been extracted for output current and voltage. Two compensators have been designed to close the loop for constant-current and constant-voltage operations considering main operating regions. The performances of the designed compensators have been verified under different load conditions. It has been shown that the designed controller successfully tracks the reference output current and voltage appropriately by adjusting the switching frequency.**

***Index Terms*—proportional-integral controller, LLC converter, control, bode plot, extended describing function.**

I. Introduction

Since the Li-ion battery technologies developed to drive electric motors in Electric Vehicles (EVs) have different operating modes such as constant current and constant voltage, it is necessary to design battery chargers that can adapt its control loops to the state of charge of the battery. Recently, several studies have been conducted on reliable and efficient battery chargers for EVs and their control. Among the power converter topologies, the LLC resonant converter is one of the widely preferred topologies for battery chargers due to its zero-voltage switching operation in a wide frequency and load range. This topology is proven to achieve both high-efficiency and high-power-density designs [1]–[4]. LLC converters can obtain ZVS for zero to rated load with a low turn-off current for the primary switches, while achieving zero current switching (ZCS) for the synchronous rectifiers (SRs). Soft turn-on and turn-off features allow minimizing the electromagnetic interference [2]. However, as it is controlled with a variable switching frequency, control of LLC resonant converter remains as a difficult task, particularly for varying loads such as batteries in electric vehicles [5].

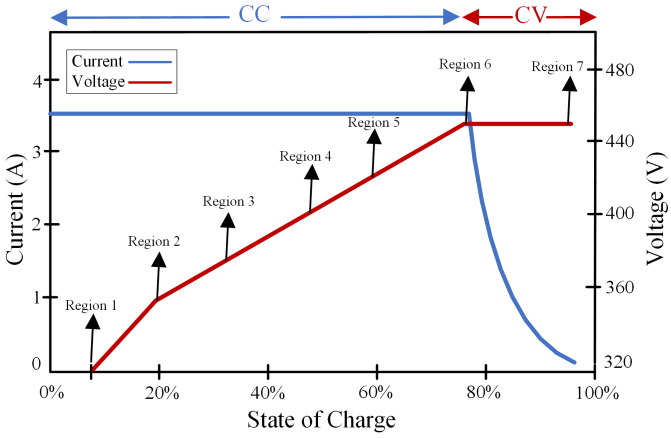

Fig. 1. Typical charging characteristics of a Li-ion battery cell.

Since a regulated output is desired in both PWM converters and resonant converters, a feedback loop is included in the control system to stabilize the system and regulate the output voltage or current. In general, small signal equivalent circuit models are used to design a robust control system for all converter structures. There are many approaches using small signal equivalent circuit models for PWM converters such as voltage mode control [6], [7], current mode control including inductor current sideband [8]–[11], V^2 control including both inductor current sideband and capacitor voltage sideband [12]–[14]. Since some state variables do not have dc components and contain switching frequency harmonics, the state-space averaging method is not preferred for resonant converters. Owing to the oscillations that occur in resonance situations, the

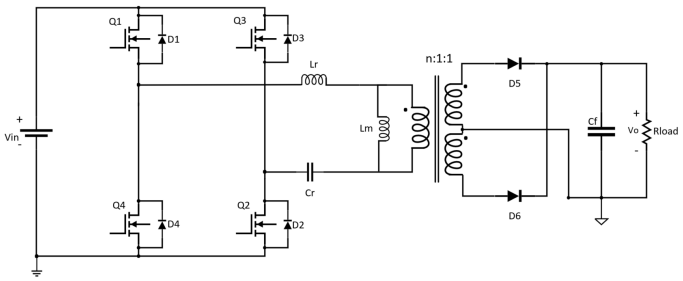

Fig. 2. Fundamental topology of LLC resonant converter.

switching frequency interacts with the resonance frequency. This is explained with the beat frequency dynamics, where a pair of double-poles located at the beat frequency determines the high frequency response [15]. Therefore, using an extended describing function method that considers the states of the resonance frequency relative to the switching frequency provides the most successful approach for a robust LLC controller design [16].

Constant current (CC) and constant voltage (CC) charging is a commonly used charging strategy for battery charging applications. The charging characteristic of a single Li-ion battery cell is shown in Fig. 1. As shown in Fig. 1, there are several key points in the charging process, namely, Region 1 to Region 7. Region 1 and Region 7 correspond to the beginning and end of the charging process, respectively. At the Region 4, the battery voltage is equal to the nominal voltage of the battery pack. The Region 6 marks the transition from CC to CV charging mode [17].

As seen from Fig. 1, the dynamic response of LLC converter in battery charger changes with respect to these operation points. This requires a closed control system design that takes into account the battery current and battery voltage separately in the battery charging application.

This paper proposes a closed-loop control for an LLC resonant converter, shown in Fig. 2, designed for battery charging applications, in which the output current and output voltage are both considered. Extended describing function method considering the states of the resonance elements relative to the switching frequency for equivalent circuit approximation has been proposed for modeling LLC converter. Thus, a simple third order equivalent circuit model of the LLC resonant converter was obtained and the beat frequency dynamics and small signal behavior of the converter were very well predicted with this circuit model. A proportional-integral control has been applied to the each transfer function.

II. Extended Describing Function Modelling of LLC Converter

The dynamic response of LLC converter changes with respect to the operation points of LLC namely, "below", "at" and "above" resonance conditions. The simple equivalent circuit model is derived based on and simplification of extended describing function method with some necessary modification

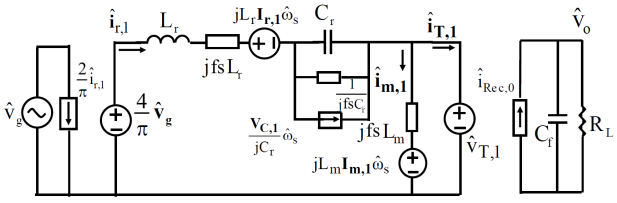

Fig. 3. Small signal model of LLC for $f_s > f_o$ [18].

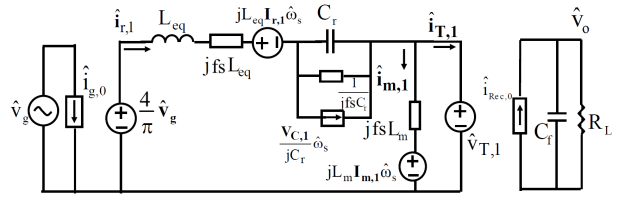

Fig. 4. Small signal model of LLC for $f_s < f_o$ [18].

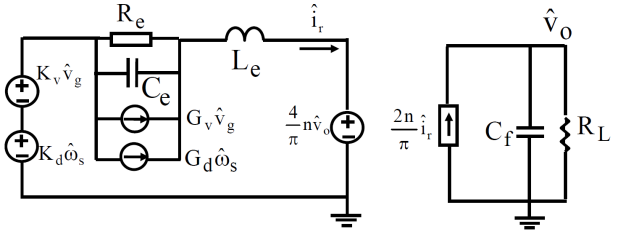

Fig. 5. Unified equivalent circuit model of LLC [18].

for the case when switching frequency F_s is below resonant frequency F_o. Therefore, the small-signal model of LLC converter is derived for both above and below resonance condition as shown in Fig. 3 and Fig. 4, respectively [16]. In Fig. 5, the small-signal models of above and below resonance frequency are combined and a simplified unified equivalent circuit is obtained. Here, L_e, R_e, C_e represent the beat frequency dynamics, K_v, G_v, K_d and G_d are the coefficients which are dependent on the magnetizing inductance L_m, L_r is in series resonant inductance, Q is quality factor and n is turn ratio of transformer [16]. These expressions are given in (1)–(10).

$$\omega_n = \frac{f_s}{f_o}, L_n = \frac{L_m}{L_r}, Q = \frac{\sqrt{L_r/C_r}}{n^2 \cdot R_L} \tag{1}$$

$$G_d = \frac{4V_g}{\pi}\frac{L_n}{\omega_o}\frac{1}{R_e} \cdot U_d \tag{2}$$

$$U_d = \frac{\frac{1}{\omega_n}\left(\frac{1}{\omega_n^2} - \omega_n^2\right)\left(\frac{\pi^2}{8}QL_n\right)^2 - \left(L_n + 1 - \frac{1}{\omega_n^2}\right)\left(\frac{2}{\omega_n^3}\right)}{\left[\sqrt{\left(L_n + 1 - \frac{1}{\omega_n^2}\right)^2 + \left(\left(\frac{1}{\omega_n} - \omega_n\right)\frac{\pi^2}{8}QL_n\right)^2}\right]^3} + \frac{2}{L_n^2} \tag{3}$$

$$K_v = \frac{8}{\pi^2}\frac{V_g L_n \omega_n}{R_{eq}} \cdot Y_V \tag{4}$$

$$Y_V = \frac{L_n + 1 - \frac{1}{\omega_n^2}}{\sqrt{\left(L_n + 1 - \frac{1}{\omega_n^2}\right)^2 + \left(\left(\frac{1}{\omega_n} - \omega_n\right)\frac{\pi^2}{8} Q L_n\right)^2}} \quad (5)$$

$$K_d = -\frac{8V_g}{\pi}\frac{1}{\omega_o L_n}, G_v = \frac{2}{\pi}\frac{X_{eq}}{\sqrt{X_{eq}^2 + R_{eq}^2}} \quad (6)$$

$$R_{eq} = \frac{8}{\pi^2} n^2 R_L, X_{eq} = f_s L_r - \frac{1}{f_s C_r} \quad (7)$$

$$L_e = \begin{cases} \left(1 + \frac{1}{\omega_n^2}\right) L_r & \text{for } \omega_n \geq 1 \\ \left(1 + \frac{1^2}{\omega_n}\right) L_r + (1 - \omega_n) L_m & \text{for } \omega_n < 1 \end{cases} \quad (8)$$

$$R_e = \begin{cases} \frac{L_e |X_{eq}||f_s - f_o|}{R_{eq}} & \text{for } \omega_n \geq 1 \\ 0 & \text{for } \omega_n \leq 1 \end{cases} \quad (9)$$

$$C_e = \frac{1}{L_e (f_s - f_o)^2} \quad (10)$$

The equation of the unified equivalent circuit is expressed in terms of the perturbations in output voltage, input voltage, resonant current, output current and switching frequency [17], [18]. In order to find the expression for i_r, superposition is applied to the equivalent circuits as in (11)–(17).

$$-K_d \cdot \widehat{w}_S + I_1 \cdot \left(\frac{R_e}{SC_eR_e + 1} + sL_e\right) = 0 \quad (11)$$

$$-K_v.\hat{v}_g + I_2 \cdot \left(\frac{R_e}{sC_eR_e + 1} + sL_e\right) = 0 \quad (12)$$

$$I_3 \cdot \left(\frac{R_e}{sC_eR_e + 1} + sL_e\right) + \frac{4}{\pi} \cdot a \cdot \hat{v}_o = 0 \quad (13)$$

$$G_v.\hat{v}_g \cdot \frac{\left(\frac{R_e}{sC_eR_e+1}\right)}{\left(\frac{R_e}{sC_eR_e+1} + sL_e\right)} = I_4 \quad (14)$$

$$G_d \cdot \widehat{w}_s \cdot \frac{\left(\frac{R_e}{sC_eR_e+1}\right)}{\left(\frac{R_e}{sC_eR_e+1} + sL_e\right)} = I_5 \quad (15)$$

$$\hat{i}_r = I_1 + I_2 + I_3 + I_4 + I_5 \quad (16)$$

$$\hat{l}_r = \frac{(K_d \cdot \widehat{w}_s + K_v \cdot \hat{v}_g)}{\left(\frac{R_e}{SC_eR_e+1} + sL_e\right)} - \frac{4}{\pi} \cdot \frac{a \cdot \hat{v}_o}{\left(\frac{R_e}{SC_eR_e+1} + sL_e\right)} + \frac{\left(\frac{R_e}{SC_eR_e+1}\right)}{\left(\frac{R_e}{SC_eR_e+1} + sL_e\right)} \cdot (G_v \cdot \hat{v}_g + G_d \cdot \widehat{w}_s) \quad (17)$$

After finding the small signal expression of i_r, the relationships of output voltage and current can be found by

$$\hat{v}_o = \frac{2a}{\pi} \cdot \hat{i}_r \cdot \frac{R_L}{sC_fR_L + 1} \quad (18)$$

$$\hat{i}_r = \hat{i}_o \cdot \left(\frac{1 + sC_f}{R_L} \cdot \frac{\pi}{2a}\right) \quad (19)$$

A simplified notation for the output current can be written as below.

$$\hat{i}_o(s) \approx G_{vg}(s)\hat{v}_g(s) + G_{vs}\widehat{\omega}_s(s) + G_{vo}(s)\hat{v}_o(s) \quad (20)$$

$$G_{vg} = \left.\frac{\hat{i}_o(s)}{\hat{v}_g(s)}\right|_{\hat{v}_o=0,\widehat{\omega}_s=0} \quad (21)$$

$$G_{vs} = \left.\frac{\hat{i}_o(s)}{\widehat{\omega}_s(s)}\right|_{\hat{v}_g=0,\hat{v}_o=0} \quad (22)$$

$$G_{vo} = \left.\frac{\hat{i}_o(s)}{\hat{v}_o(s)}\right|_{\hat{v}_g=0,\widehat{\omega}_s=0} \quad (23)$$

The control block diagram of the LLC resonant converter with a CC and CV regions are shown in Fig. 6. The transfer function of $\hat{v}_o/\widehat{\omega}_s$ for the CV region and the transfer functions of $\hat{i}_o/\widehat{\omega}_s$ for the CC region are given in (24)–(25).

$$\frac{\hat{v}_o}{\widehat{w}_s} = \frac{\left(\frac{K_d + \left(\frac{R_e}{sC_eR_e+1}\right) \cdot G_d}{\left(\frac{R_e}{sC_eR_e+1} + sL_e\right)}\right)}{\left(\frac{sC_fR_L+1}{R_L} \cdot \frac{\pi}{2a} + \frac{4}{\pi} \cdot \frac{a}{\left(\frac{R_e}{sC_eR_e+1} + sL_e\right)}\right)} \quad (24)$$

$$\frac{\hat{i}_o}{\widehat{w}_s} = \frac{\left(\frac{K_d + \left(\frac{R_e}{sC_eR_e+1}\right) \cdot G_d}{\left(\frac{R_e}{sC_eR_e+1} + sL_e\right)}\right)}{\left(1 + \frac{8R_La^2}{\left(\frac{R_e}{sC_eR_e+1} + sL_e\right) \cdot (sC_fR_L+1) \cdot \pi^2}\right) \cdot \left(\frac{1+sC_f}{R_L} \cdot \frac{\pi}{2a}\right)} \quad (25)$$

III. Compensator Design and Results

For a battery charging application with specifications of 370V-430V/36V-54V 3700W LLC converter with resonance frequency of 400 kHz, the magnetization inductance, resonant inductance, and resonant capacitor of $34.7\ \mu H$, $8.68\ \mu H$, and $18.25\ nF$, respectively, were considered in this study.

In order for the control loop system to operate at CC operating points effectively, the system was designed according to the Region 4 condition 400V/48V 3288W with 405kHz switching frequency. For the CV region, the control system was designed according to Region 6 400V/54V 3700W with 325kHz switching frequency.

The obtained transfer functions for the CC and CV regions were given in (26)-(27) for Region 4 and Region 6 respectively. Fig. 7 and Fig. 8 show the open loop Bode plots for every operating region.

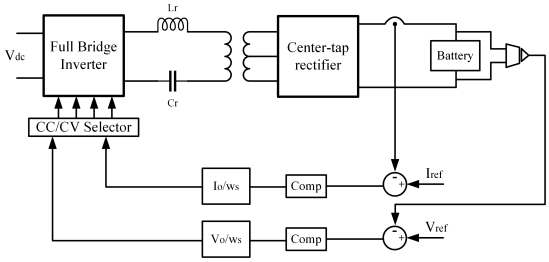

Fig. 6. Control block diagram of LLC for each region.

$$\frac{\hat{v}_o(s)}{\widehat{\omega}_s(s)} = \frac{-\left(9.893 \times 10^{11}\right)}{(8.153)s^3 + \left(1.729 \times 10^7\right)s^2 + \left(1.072x10^{11}\right)s + \left(1.045 \times 10^{17}\right)} \tag{26}$$

$$\frac{\hat{i}_o(s)}{\widehat{\omega}_s(s)} = \frac{-\left(1.413 \times 10^{12}\right)}{(8.153)s^3 + \left(1.729 \times 10^7\right)s^2 + \left(1.072 \times 10^{11}\right)s + \left(1.045 \times 10^{17}\right)} \tag{27}$$

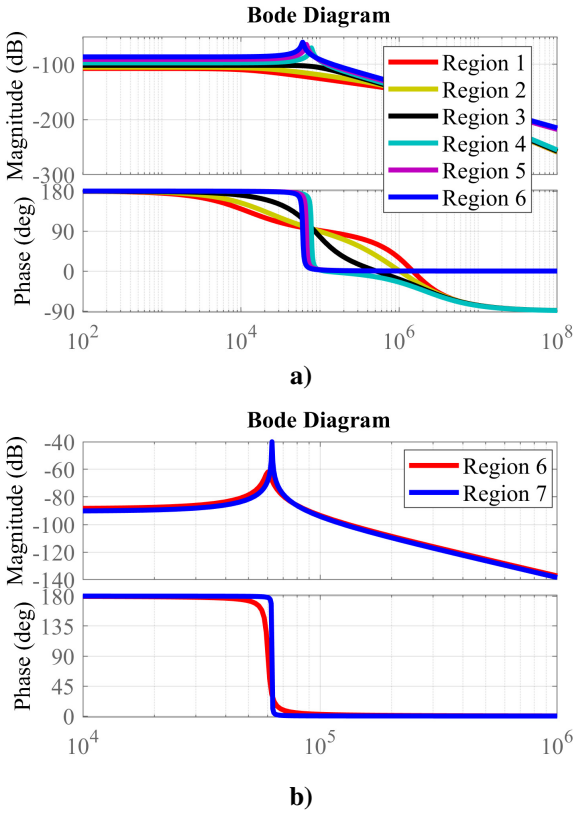

Fig. 7. Bode diagram of transfer functions **a)** $\hat{\imath}_o/\widehat{\omega}_s$, **b)** $\hat{v}_o/\widehat{\omega}_s$.

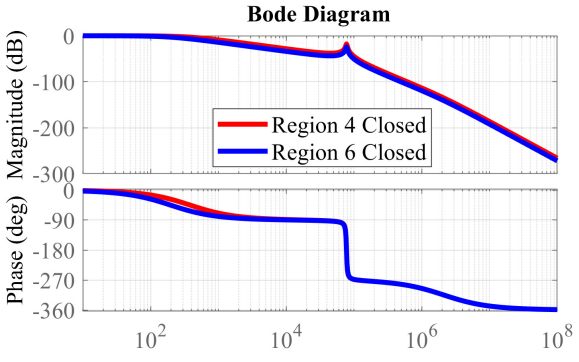

Fig. 8. Bode diagram of closed loop Region 4 and Region 6.

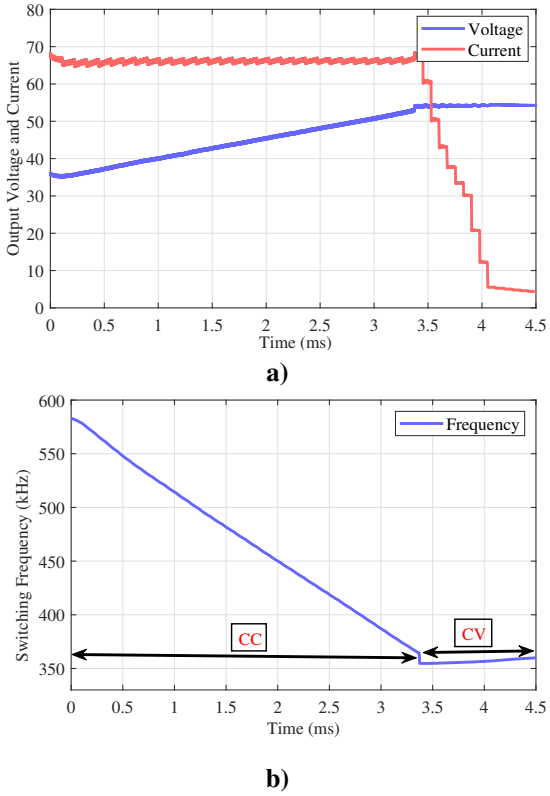

Fig. 9. Battery charger results of **a)** output voltage and current **b)** switching frequency variation.

By using the obtained transfer functions, the closed-loop equivalent transfer function of the system is obtained for CC and CV region, and the transfer functions of the designed integral compensator were $I_{i_o} = -28190666$ and $I_{v_o} = -20750500$ respectively. Several simulations were performed by setting references with different frequencies at the control input, measuring the system response and calculating its magnitude and phase by means of open PID Tuner in MATLAB environment. The control loop is composed of only an integral (I) compensator. The reason why the integral compensator gain was achieved so large is the amount of switching frequency. The bode diagrams of the closed loop transfer functions are shown in Fig. 8.

Fig. 9(a) shows the response of the CC and CV control

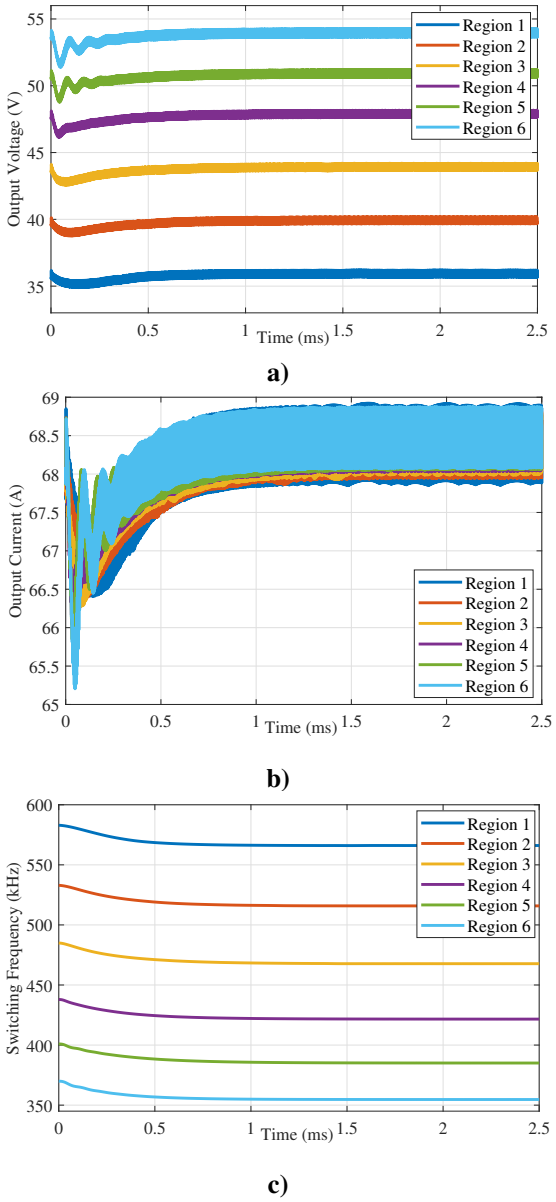

Fig. 10. Different load condition results in CC region **a)** output voltage, **b)** output current, **c)** switching frequency.

loops according to the given load profile. The whole charging process has been shortened to 5ms to save the simulation time. In the CC region, the closed loop current controller successfully regulates the current at 68A. In the CV region, the closed loop CV controller is activated and battery voltage is regulated at 54V, while the current slowly decreases as battery is being charged. The variation of the control variable switching frequency with respect to the varying load profile is shown in Fig. 9(b). The system starts with high switching frequency and the frequency decreases as the battery is being charged.

The control structure designed according to certain operating points should be able to perform well and track the reference output voltages and currents under different operating points and instantaneous loading conditions. Fig. 10(a)-(b) shows the response of the CC control loop for 6 different loading situations in favor of the output voltage and currents. These curves represent the worst loading conditions for each operating point where 68A reference was provided to the controller from a reference of 0 A. As it can be seen from Fig. 10(c), the controller ensures a stable system by adjusting the switching frequency to below or above the resonance frequency in different load conditions.

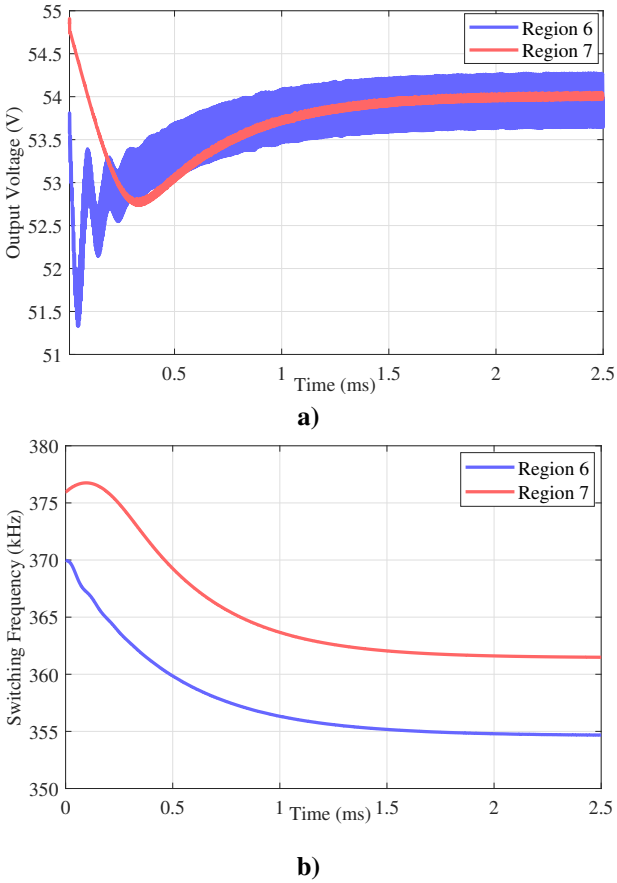

Fig. 11. Different load condition results in CV region **a)** output voltage, **b)** switching frequency variation.

Fig. 11(a) shows that the designed control structure ensures regulated output voltage. Likewise, the control variable switching frequency variation under different load conditions in CV region is shown in Fig. 11(b).

IV. Conclusion

In this study, a CC and CV control scheme for a LLC resonant converter was presented in detail for battery charging applications. The small-signal model of the LLC converter is derived for both above and below resonance condition in order to obtain more accurate dynamic model.

A simple third order equivalent circuit model of the LLC resonant converter was derived and the beat frequency dynamics and small signal behavior of the converter were very well predicted with this circuit model.

The designed compensators for CC and CV operations at output voltage of 48V and 54V, respectively, have been simulated at different operating points. It has been shown that the output current and voltage references have been successfully tracked for whole load profiles.

ACKNOWLEDGMENT

This paper has been produced benefiting from the H2020-MSCA-IF-2020 (Project No: 101031029) and the 2232 International Fellowship for Outstanding Researchers Program of TUBITAK (Project No: 118C374). However, the entire responsibility of the paper belongs to the owner of the paper. The financial support received from TUBITAK does not mean that the content of the publication is approved in a scientific sense by TUBITAK..

REFERENCES

[1] Bo Yang, F. C. Lee, A. J. Zhang and Guisong Huang, "LLC resonant converter for front end DC/DC conversion," APEC. Seventeenth Annual IEEE Applied Power Electronics Conference and Exposition, Dallas, TX, USA, 2002, pp. 1108-1112 vol.2.

[2] F. C. Lee, Shuo Wang, Pengju Kong, Chuanyun Wang and Dianbo Fu, "Power architecture design with improved system efficiency, EMI and power density," 2008 IEEE Power Electronics Specialists Conference, Rhodes, Greece, 2008, pp. 4131–4137.

[3] H. Wang, S. Dusmez and A. Khaligh, "Design and Analysis of a Full-Bridge LLC-Based PEV Charger Optimized for Wide Battery Voltage Range," in IEEE Transactions on Vehicular Technology, vol. 63, no. 4, pp. 1603-1613, May 2014.

[4] H. Wang, S. Dusmez and A. Khaligh, "Maximum Efficiency Point Tracking Technique for LLC-Based PEV Chargers Through Variable DC Link Control," in IEEE Transactions on Industrial Electronics, vol. 61, no. 11, pp. 6041-6049, Nov. 2014

[5] Y. Shen, W. Zhao, Z. Chen and C. Cai, "Full-Bridge LLC Resonant Converter With Series-Parallel Connected Transformers for Electric Vehicle On-Board Charger," in IEEE Access, vol. 6, pp. 13490-13500, 2018.

[6] R. Tymerski, V. Vorperian, F. C. Y. Lee and W. T. Baumann, "Nonlinear modeling of the PWM switch," in IEEE Transactions on Power Electronics, vol. 4, no. 2, pp. 225-233, April 1989.

[7] V. Vorperian, "Simplified analysis of PWM converters using model of PWM switch. Continuous conduction mode," in IEEE Transactions on Aerospace and Electronic Systems, vol. 26, no. 3, pp. 490-496, May 1990.

[8] J. Li and F. C. Lee, "New Modeling Approach and Equivalent Circuit Representation for Current-Mode Control," in IEEE Transactions on Power Electronics, vol. 25, no. 5, pp. 1218-1230, May 2010.

[9] Y. Yan, F. C. Lee and P. Mattavelli, "Unified Three-Terminal Switch Model for Current Mode Controls," in IEEE Transactions on Power Electronics, vol. 27, no. 9, pp. 4060-4070, Sept. 2012.

[10] Shuilin Tian, F. C. Lee, J. Li, Q. Li and P. -h. Liu, "Equivalent circuit model of constant on-time current mode control with external ramp compensation," 2014 IEEE Energy Conversion Congress and Exposition (ECCE), Pittsburgh, PA, USA, 2014, pp. 3747-3754.

[11] S. Tian, F. C. Lee, J. Li, Q. Li and P. Liu, "A Three-Terminal Switch Model of Constant On-Time Current Mode With External Ramp Compensation," in IEEE Transactions on Power Electronics, vol. 31, no. 10, pp. 7311-7319, Oct. 2016.

[12] J. Li and F. C. Lee, "Modeling of V^2 Current-Mode Control," in IEEE Transactions on Circuits and Systems I: Regular Papers, vol. 57, no. 9, pp. 2552-2563, Sept. 2010.

[13] S. Tian, F. C. Lee, P. Mattavelli, K. Cheng and Y. Yan, "Small-Signal Analysis and Optimal Design of External Ramp for Constant On-Time V^2 Control With Multilayer Ceramic Caps," in IEEE Transactions on Power Electronics, vol. 29, no. 8, pp. 4450-4460, Aug. 2014.

[14] S. Tian, F. C. Lee, Q. Li and Y. Yan, "Unified Equivalent Circuit Model and Optimal Design of V^2 Controlled Buck Converters," in IEEE Transactions on Power Electronics, vol. 31, no. 2, pp. 1734-1744, Feb. 2016.

[15] V. Vorperian, "Approximate small-signal analysis of the series and the parallel resonant converters," in IEEE Transactions on Power Electronics, vol. 4, no. 1, pp. 15-24, Jan. 1989.

[16] S. Tian, F. C. Lee and Q. Li, "Equivalent Circuit Modeling of LLC Resonant Converter," in IEEE Transactions on Power Electronics, vol. 35, no. 8, pp. 8833-8845, Aug. 2020.

[17] H., Wang, "Highly efficient SiC based onboard chargers for plug-in electric vehicles,"PhD Thesis, University of Maryland, College Park, 2014.

[18] S. Tian, "Equivalent Circuit Model of High Frequency Pulse- Width-Modulation (PWM) and Resonant Converters," PhD Thesis, Virginia Polytechnic Institute and State University, Blacksburg, Virginia, 2015.